

Reconfigurable Photoflow Reactor for Enhanced Optimization of The Aerobic Oxidative Coupling of 2-phenylbenzoic Acid

Florian Ehrlich-Sommer,^a Tobias Friedl,^b Christian Koller,^b and Malek Y. S. Ibrahim^{*a}

^a*Redeem Solar Technologies GmbH, Sandgasse 36 / IV 8010 Graz, Austria.*

^b*University of Applied Sciences Wiener Neustadt, Johannes Gutenberg-Straße 3, 2700 Wiener
Neustadt, Austria*

E-mail: malek.ibrahim@redeemtechnologies.com

Supplementary Information

Table of Contents

1. Material and Methods.....	3
1.1. Chemicals.....	3
1.2. Characterisation	3
1.3. Photochemical oxidative coupling in the Photoflow reactor	3
1.4. Switching the configuration of the Photoflow reactor.....	5
1.5. Computational Fluid Dynamics CFD	5
2. Calculation of the apparent rate constant K.....	7
3. Testing (Config.4) and (Config.6) under different air flowrates	8
4. CFD results for (Config.4) and (Config.5)	8
5. Correlation between the apparent rate constant K and geometry parameters of the reactors	12
6. List of symbols.....	13
7. Product NMR (Crude).....	14

1. Material and Methods

1.1. Chemicals

Biphenyl-2-carboxylic acid **a1**, 8% was purchased from Thermo Scientific. 9-mesityl-10-methylacridinium perchlorate ([Acr-Mes]ClO₄) **a3** > 98% was purchased from TCI Chemicals. Acetonitrile Chromasolv gradient from Honeywell was used as a solvent. Distilled water was used as a cosolvent. Chloroform-d from Cambridge isotope was used for NMR.

1.2. Characterisation

Conversion of the starting material and product yield were quantified using Gas chromatography mass spectroscopy (GC–MS) versus mesitylene as an internal standard. GC measurements were performed on an Agilent 7890 A with an Agilent 19091J-433 column coupled to an Agilent 5975 C mass spectrometer. 2 µl aliquot was pipetted the collection vessel in case of flow reactors and diluted in 1 ml acetonitrile that contains a known amount of the mesitylene internal standard in a GC vial before being injected into the GC. The retention time of the starting material and the product are 8.239 and 9.299 min s shown in Figure S1.

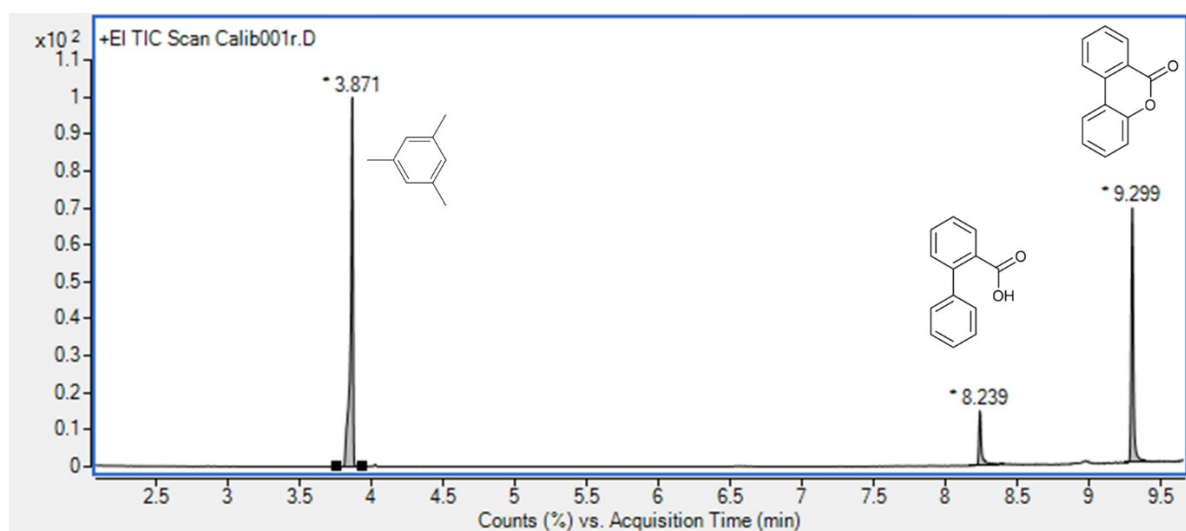


Figure S1 | GC-MS chromatogram showing the peaks for starting material, product and internal standard.

NMR spectra were recorded on Bruker Avance III 300 MHz spectrometer. Chemical shifts δ are given in ppm. ¹H NMR spectra are referenced to residual protons in the solvent to the deuterated solvent peak. The multiplicity of peaks is denoted as singlet (s), doublet (d), triplet (t), quadruplet (q), doublet of doublets (dd), doublet of doublets of doublets (ddd), doublet of triplets (dt), triplet of doublets (td), or multiplet (m).

1.3. Photochemical oxidative coupling in the Photoflow reactor

The photocatalytic oxidative coupling experiments were carried out in in a reconfigurable photo flow reactors from Redeem Solar Technologies GmbH. In all configurations, the reactor is fitted with 8 mm thick glass windows and is sealed with a fresh Viton O-rings. In all tests, the reactor was always positioned parallel to the ground except in the case of the 60-degree inclined

configuration (**Config.3**) as shown in Figure S2. Ten (10) ml solution of acetonitrile and water (4:1 v) containing 198 mg of **a1** and 0.5 mol% of the catalyst **a3** was prepared in an aluminium-covered glass vial sealed with a four outlet gas-tight Teflon cap. A peristaltic pump was used for solution circulation through the reactor and back to the collection vessel at 30 ml/min. Another pump was used to co-feed ambient air to the reactor at 1.33 ml/min. A Y-shaped micro mixer was used for mixing air with the solution before the reactor inlet.

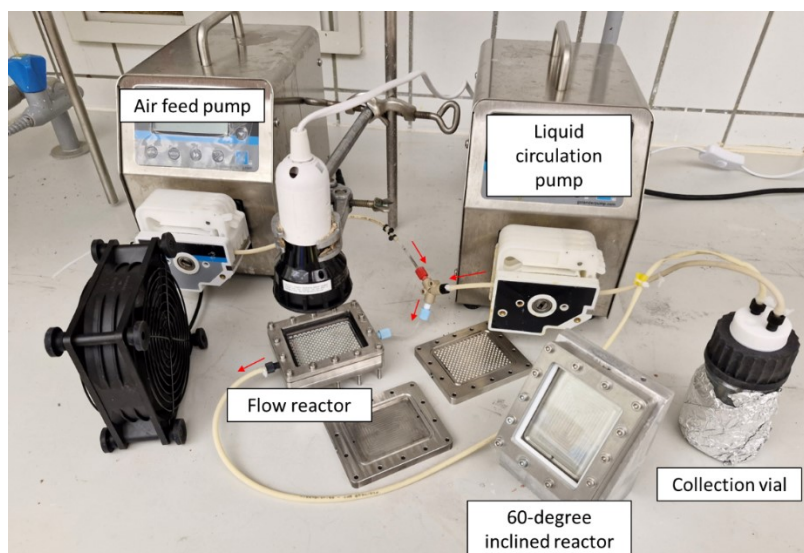


Figure S2 | Flow setup for the photocatalytic oxidative cross coupling of **1a** in different configurations.

The reactor was then illuminated with a 6200 white light from Hepatochem with illumination in the range of 400 to 750 nm, Figure S3. The light source was positioned at 4 cm from the top of the reactor window. The reactor was cooled with a cooling fan to keep its temperature between 25 and 28 °C. Light transmission through the common glass window that all the flow reactor configurations share was measured with a light meter and it was found out that the variation between the edge and the centre is less than 7%.

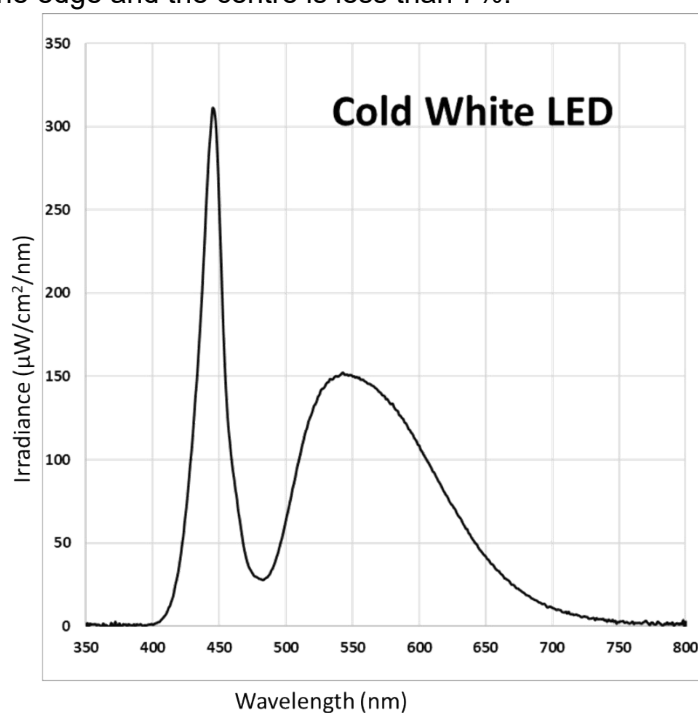


Figure S3 | intensity of the used white light source in batch and flow experiments

1.4. Switching the configuration of the Photoflow reactor

To switch between configurations of the photoflow reactor, the 14 bolts are untightened and the bottom part of the reactor which contains the flow channel is replaced by the part that has the desired configuration. A fresh O-ring is positioned and the reactor is assembled and the bolts are tightened by hand, Figure S4. The reactor is pressure tested with 5 bar of nitrogen gas before testing. To test the reactor, the inlet and outlet fittings are tightened and the reactor is positioned under the light source.

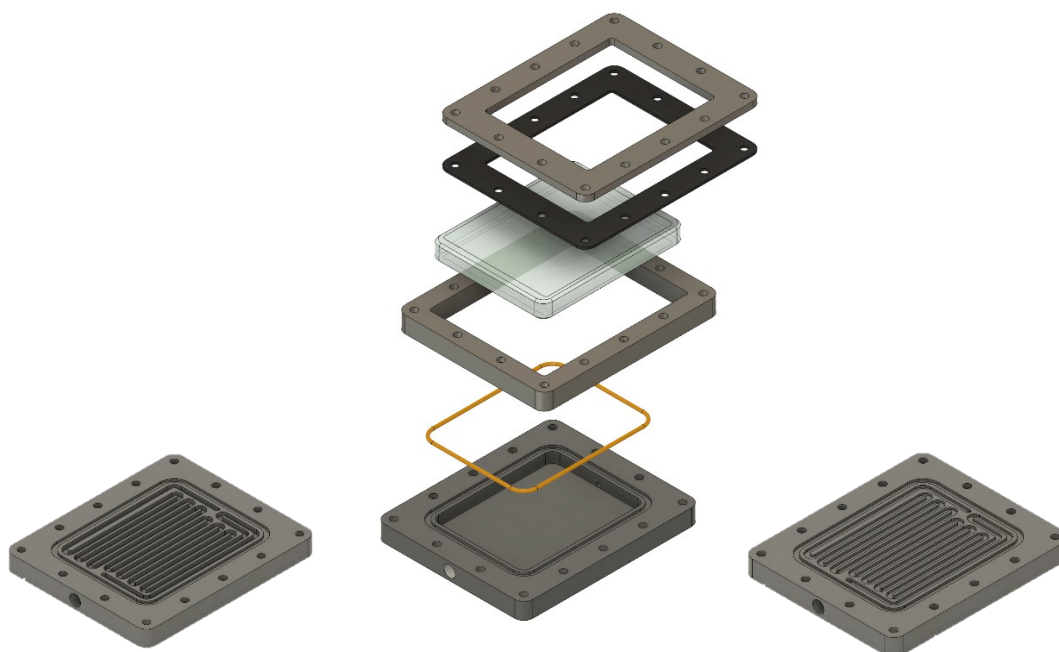


Figure S4 | assembly of reconfigurable photoflow reactor

1.5. Computational Fluid Dynamics CFD

CFD was carried out to estimate the effective flow cross section area for (**Config.4, and 5**) The following equations have been taken from the Laminar Flow interface inside COMSOL Multiphysics® for an incompressible fluid with gravity acting on it. These equations were set up through RANS formulations and the k - ϵ turbulence model.

In this set of equation the variables solved for are the turbulent kinetic energy k and the turbulent dissipation ϵ . The other, intermediate variables that need to be solved are the turbulent viscosity (or eddy viscosity) μ_T and the production term P_k . The colon ($:$) in equation refers to the Frobenius inner product and in this specific case takes two tensors of second order (or matrices), acts as a component-wise inner product and returns a scalar. Thus effectively reducing the order of the resulting tensor compared to its tensor products by two.

It should be noted that C_μ , $C_{\epsilon 1}$, $C_{\epsilon 2}$, σ_k and σ_ϵ are model constants and they strongly determine how the model behaves, how turbulences are treated and what the solution will be. There is a rather standard set of these constants that multiple data fitting instances have

arrived at for many different instances of turbulent flow. This particular set is also used in COMSOL by default and is used in this work.

$$\rho(\mathbf{U} \cdot \nabla) \mathbf{U} = \nabla \cdot [-p\mathbf{I} + \mathbf{K}] + \mathbf{F} + \rho\mathbf{g}$$

$$\rho \nabla \cdot \mathbf{U} = 0$$

$$\mathbf{K} = (\mu + \mu_T) (\nabla \mathbf{U} + (\nabla \mathbf{U})^T)$$

$$\rho(\mathbf{U} \cdot \nabla) k = \nabla \cdot \left[\left(\mu + \frac{\mu_T}{\sigma_k} \right) \nabla k \right] + P_k - \rho \epsilon$$

$$\rho(\mathbf{U} \cdot \nabla) \epsilon = \nabla \cdot \left[\left(\mu + \frac{\mu_T}{\sigma_\epsilon} \right) \nabla \epsilon \right] + C_{\epsilon 1} \frac{\epsilon}{k} P_k - C_{\epsilon 2} \rho \frac{\epsilon^2}{k}$$

$$\mu_T = \rho C_\mu \frac{k^2}{\epsilon}$$

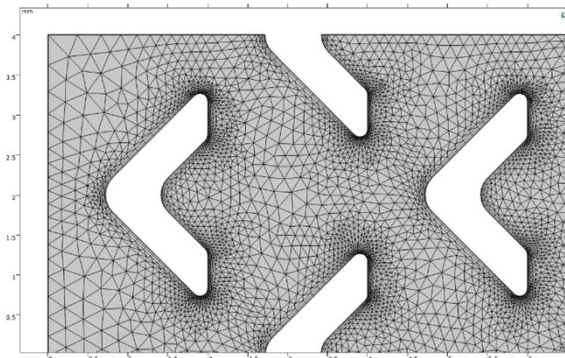
$$P_k = \mu_T [\nabla \mathbf{U} : (\nabla \mathbf{U} + (\nabla \mathbf{U})^T)]$$

The constants are as follows:

$$C_\mu = 0.09 \quad | \quad C_{\epsilon 1} = 1.44 \quad | \quad C_{\epsilon 2} = 1.92 \quad | \quad \sigma_k = 1.0 \quad | \quad \sigma_\epsilon = 1.3$$

The fully developed flow condition is here declared as a volumetric flow rate $Q_{in} = 833$ [mm³/s]. A built in function for an automatic mesh generation in COMSOL is used. This feature has options to optimize the mesh for solving one or more specific parts of physics that are used in the model. The only physics-module used in the present case is the Laminar Flow module, which the mesh will be generated for with standard mesh size.

Turbulence models that expand the Navier-Stokes equations through an additional term to represent turbulent eddy viscosity where compared to the laminar model. The turbulence models include Algebraic y-Plus, L-VEL, k- ϵ and Low Reynolds Number k- ϵ .



. Figure S5 | Standard mesh for CFD simulation

2. Calculation of the apparent rate constant K

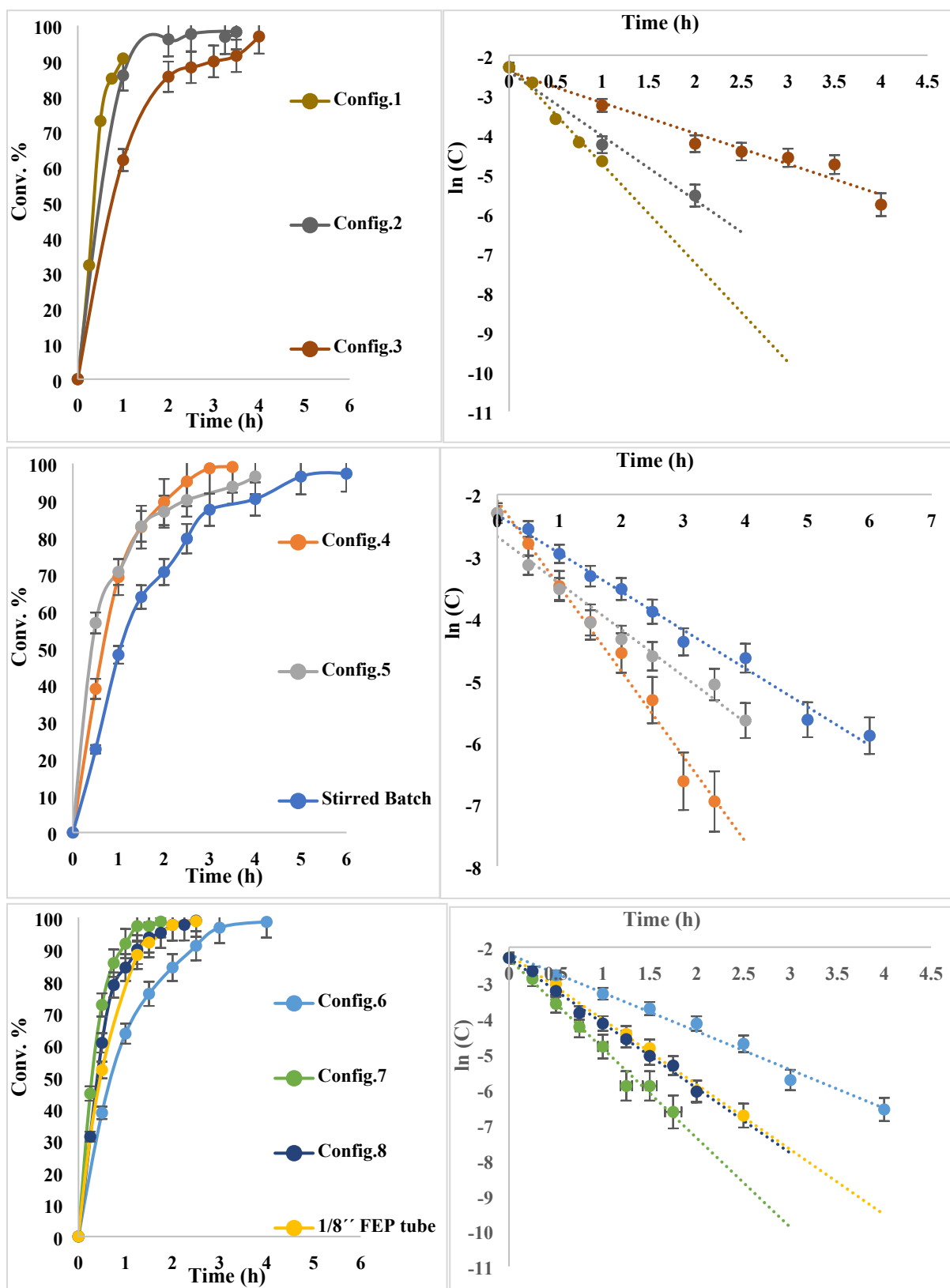
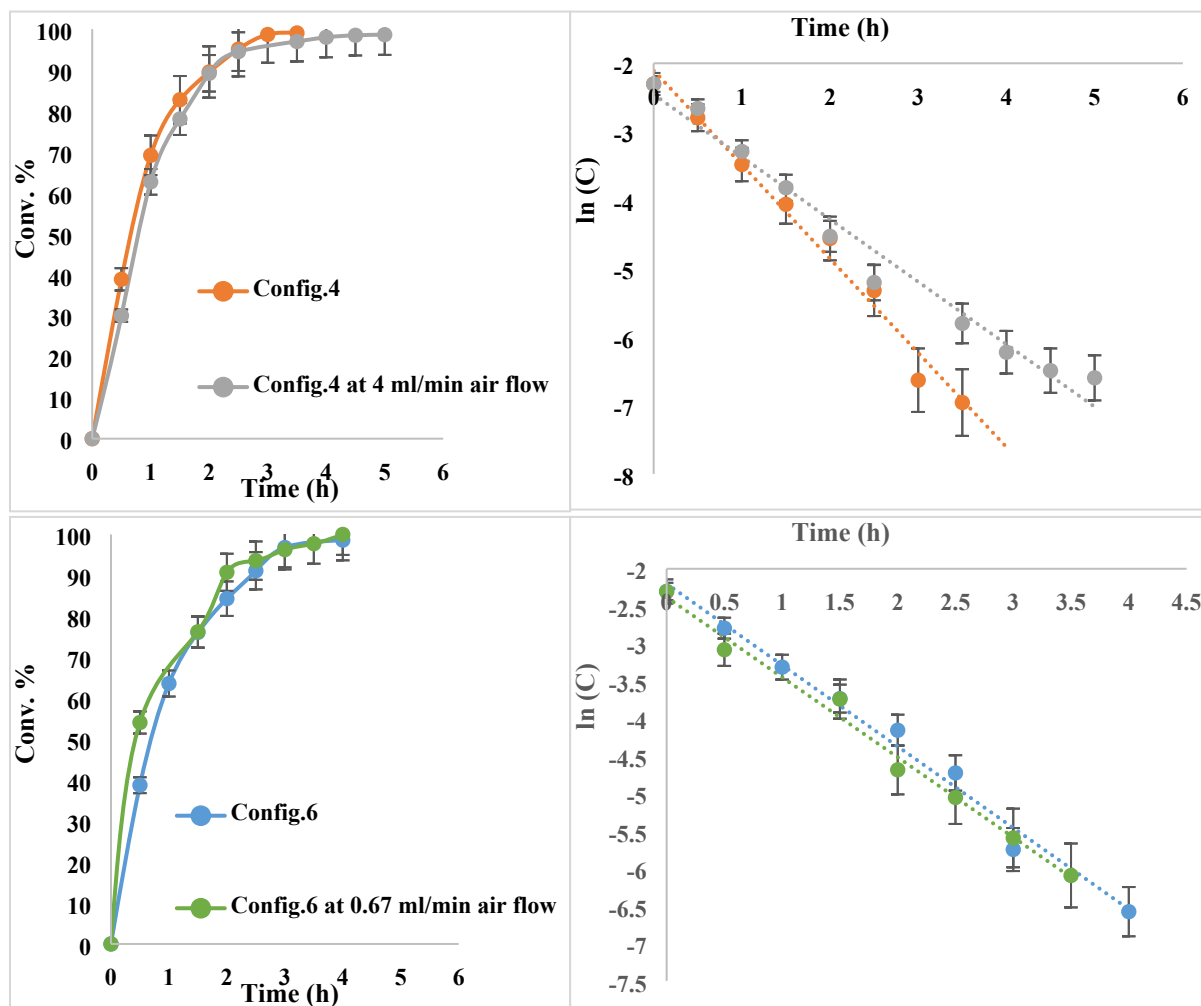


Figure S6 | Concentration profile of the starting material **a1** with time and the calculated first order apparent rate constant K for the tested photoreactors.

3. Testing (Config.4) and (Config.6) under different air flowrates

The air flow rate was changed by changing the setpoint on the air feed pump while the reaction setup remained the same as explained in Section SI 1.3 with (Config.4, and 6)



4. CFD results for (Config.4) and (Config.5)

The velocity magnitude for a laminar flow regime for (**Config.4**) in the cut structure is shown. The peak velocity resides in the deep red parts and numbers close to 55 [mm/s]. So theoretically, a fluid particle that perfectly follows the highest velocity streamline in this flow would approximately take one second to get from the inlet to the outlet. This minimum residence time is suspected to become longer with the addition of turbulence and the simulation of the boxes at the inlet. Furthermore, it is already noticeable that the areas directly behind the arrowheads do not experience much flow through them. It is entirely possible that fluid reside there for a comparatively long time. The difference in flow velocity between the channels/streams with high velocity and the areas with low velocity is highlighted as a line graph of the cross section in between two rows of arrowheads. From this graph, the average velocity is calculated to be **37.5 mm/s** which results in a calculated flow cross section to equal **22.2 mm²** from the specified total volumetric flow in the CFD.

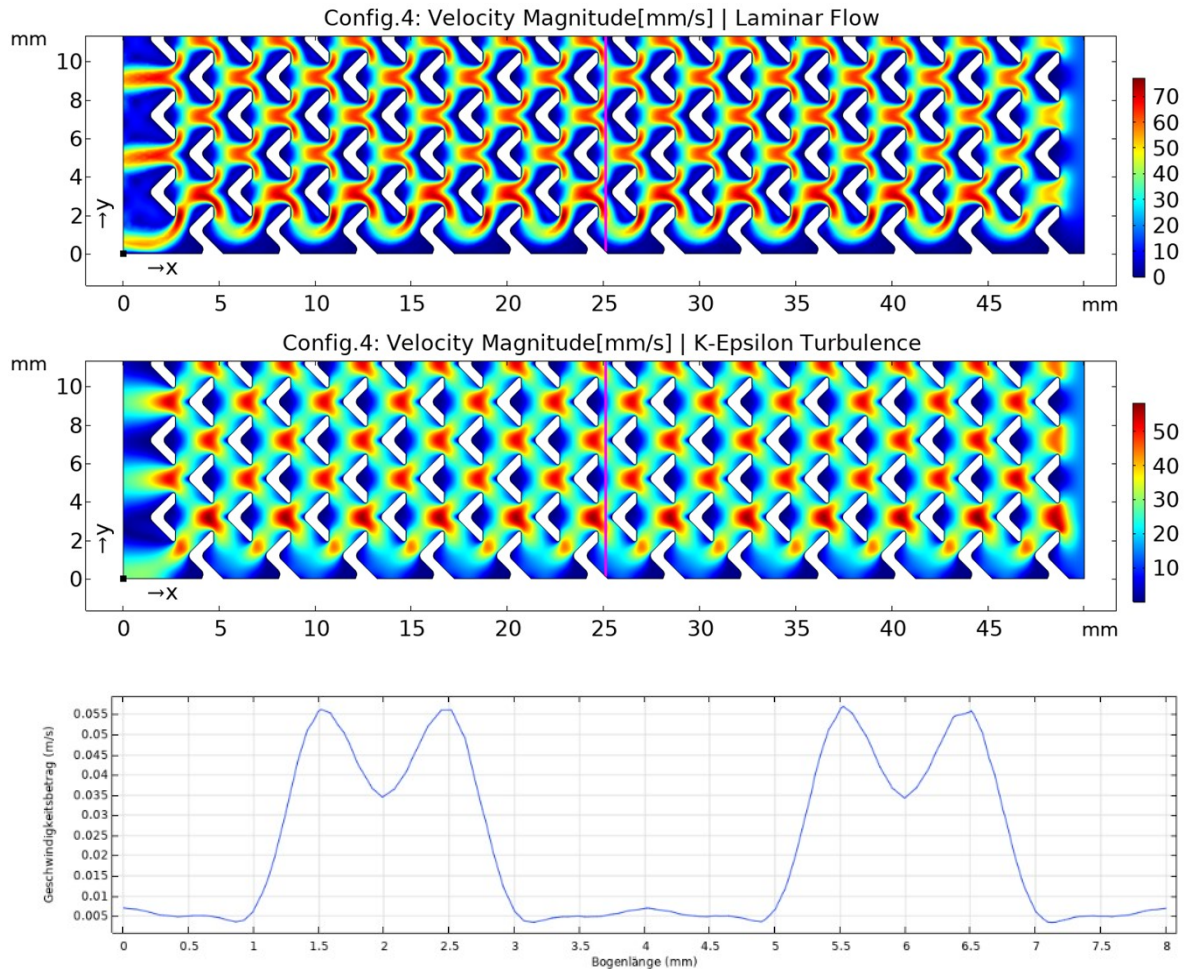


Figure S8 | Velocity magnitude map for laminar (top) and k-epsilon turbulence model(middle) and velocity profile across two arrows (bottom) for **Config.4**.The velocity profile is take at the purple line indicated on the velocity map.

The turbulence models Algebraic yPlus, L-VEL and LowRe k-epsilon show basically identical results to the laminar flow solution. The k- ϵ model solves for the turbulent kinetic energy (k) and the rate of dissipation of turbulent kinetic energy (ϵ). Wall functions are used to approximate the behavior of fluid flow in the buffer region instead of simulating it. This model is often used because of its high rate of convergence and comparatively low memory demand. It has problems accurately computing situations where stark pressure gradients, curvature of flow or jet flow are present. The Low Reynolds k- ϵ model is an extension of the k- ϵ model and does not use wall functions, it solves for the flow everywhere. Because the data was different between laminar and k-epsilon turbulence model we decided to show both results to indicate the effect of turbulence.

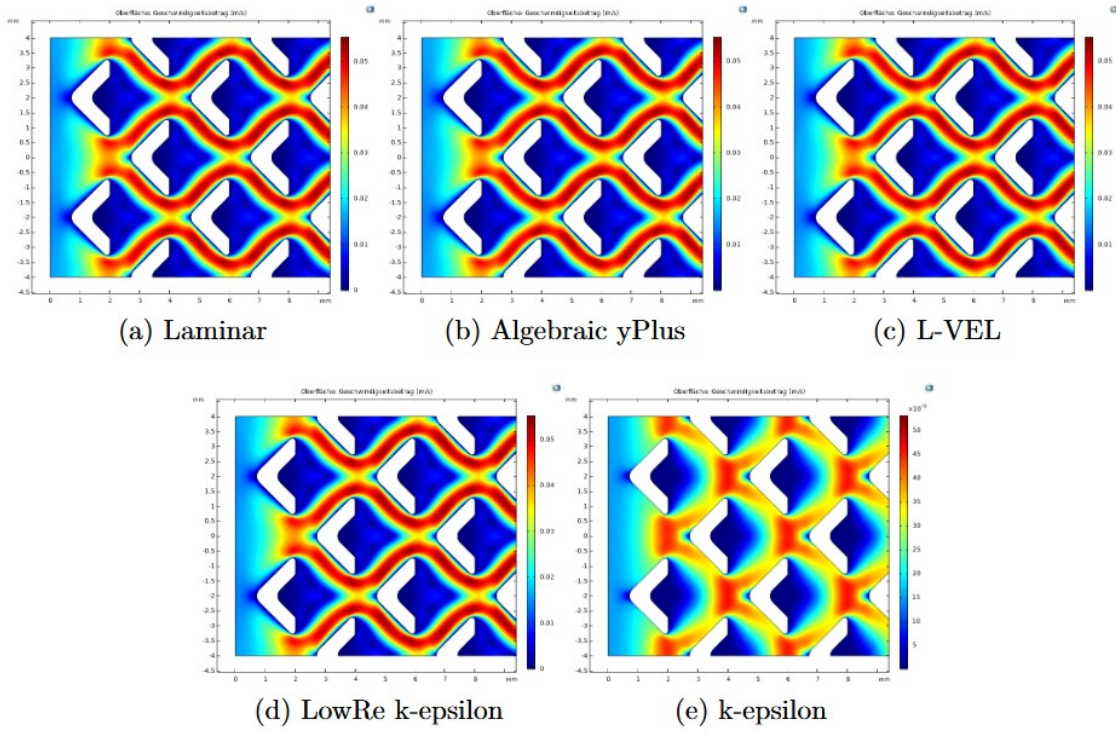


Figure S9 | Comparison of the Velocity magnitude map for **Config.4** with laminar and different turbulence models.

For **Config.5**, the flow already covers a much larger area when creeping through the border regions compared to both the laminar and turbulent flows in (**Config.4**). A small disadvantage are the no-flow areas to the sides of the arrowhead's tips in the entire geometry. When comparing laminar to k-epsilon turbulence model for this configuration, it can be seen that turbulence forces the flow closer to the arrow borders and result in smaller zones with low- or no-flow. The calculated average velocity is **26 mm/s** which corresponds to a flow cross section area that equals **32 mm²**.

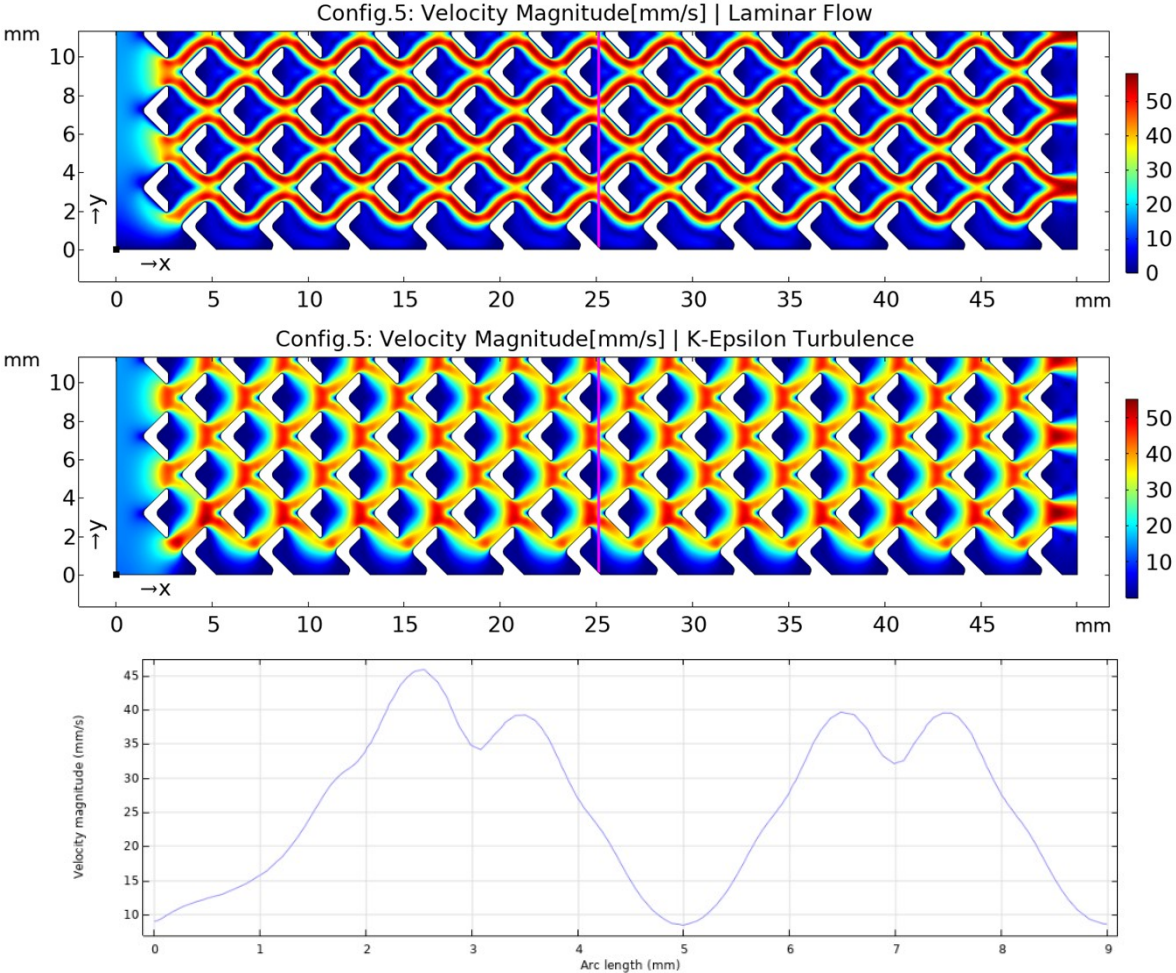


Figure S10 | Velocity magnitude map for laminar (top) and k-epsilon turbulence model(middle) and velocity profile across two arrows (bottom) for **Config.5**. The velocity profile is take at the purple line indicated on the velocity map.

5. Correlation between the apparent rate constant K and geometry parameters of the reactors

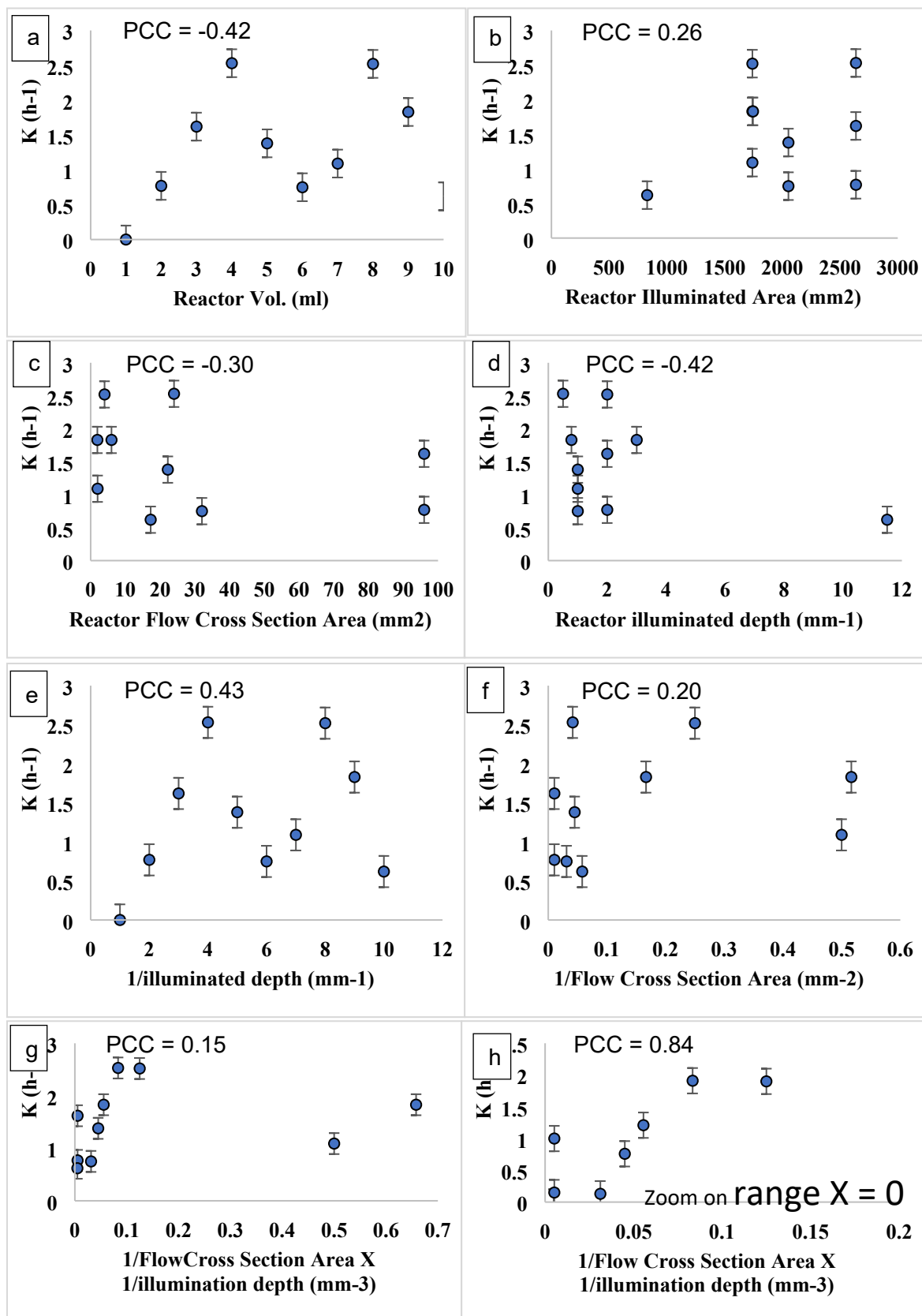


Figure S11 | Correlation plots between the apparent rate constant K and different geometrical parameters of the tested photo reactors. (a) correlation with reactor volume, (b) correlation with the reactor illuminated area i.e. area perpendicular on the incident photon flux on the reaction fluid, (c) correlation with the reactor flow cross section

area i.e. area perpendicular on the direction of fluid flow, (d) correlation with the reactor illuminated depth i.e. the distance that light needs to penetrate to shin at the bottom of the reactor channel, (e) correlation with the inverse of the reactor illuminated depth i.e. the distance that light needs to penetrate to shin at the bottom of the reactor channel, (f) correlation with the inverse of the reactor flow cross section area i.e. area perpendicular on the direction of fluid flow, (g) correlation with the multiplication of the inverse of the reactor flow cross section area i.e. area perpendicular on the direction of fluid flow and the inverse of the reactor illuminated depth i.e. the distance that light needs to penetrate to shin at the bottom of the reactor channel, (h) zoom in on subplot g to show correlation in the range of x between 0 and 0.2. **PCC** is Pearson Correlation Coefficient.

6. List of symbols

Symbol	Definition	Unit
ρ	fluid density	kg/m^3
\mathbf{u}	fluid velocity vector	m/s
p	fluid pressure	Pa
μ	fluid dynamic viscosity	$Pa \cdot s$
D/Dt	substantial/material derivative	1
K	viscous stress tensor	Pa
S	strain-rate tensor	s^{-1}
\mathbf{U}	time-averaged fluid velocity vector for RANS	m/s
P	time-averaged fluid pressure for RANS	Pa
μ_T	turbulent viscosity term for RANS	$Pa \cdot s$
\mathbf{v}	particle velocity vector	m/s
m_p	solid particle mass	kg
\mathbf{F}_D	drag force	N
\mathbf{F}_g	gravitational force	N
\mathbf{F}_L	lift force	N
Re_r	relative Reynolds number	1
d_p	solid particle diameter	m
τ_p	particle velocity response time	s
ρ_p	solid particle density	kg/m^3
C_D	drag coefficient	1

7. Product NMR (Crude)

